

See discussions, stats, and author profiles for this publication at: <https://www.researchgate.net/publication/220018714>

Lithium-Doped Germanium Nanowire? Experimental and Theoretical Indication

ARTICLE *in* THE JOURNAL OF PHYSICAL CHEMISTRY C · JUNE 2009

Impact Factor: 4.77 · DOI: 10.1021/jp900950k

CITATIONS

9

READS

25

6 AUTHORS, INCLUDING:



Gopinadhanpillai Gopakumar

Max Planck Institute for Chemical Energy C...

33 PUBLICATIONS 545 CITATIONS

[SEE PROFILE](#)



Peter Lievens

University of Leuven

278 PUBLICATIONS 4,591 CITATIONS

[SEE PROFILE](#)



Minh Tho Nguyen

University of Leuven

748 PUBLICATIONS 10,846 CITATIONS

[SEE PROFILE](#)

Lithium-Doped Germanium Nanowire? Experimental and Theoretical Indication

G. Gopakumar,[†] Xin Wang,[‡] Ling Lin,[†] Jorg De Haeck,[‡] Peter Lievens,^{*,‡} and Minh Tho Nguyen^{*,†}

Department of Chemistry, Laboratory of Solid State Physics and Magnetism, and Institute for Nanoscale Physics and Chemistry (INPAC), Katholieke Universiteit Leuven, B-3001 Leuven, Belgium

Received: February 2, 2009; Revised Manuscript Received: April 22, 2009

We report a combined experimental and theoretical study of lithium-doped germanium clusters. The doped germanium clusters are produced using a dual-laser dual-target vaporization source and subsequently analyzed using a reflectron time-of-flight (RTOF) mass spectrometer. The RTOF mass spectrum showing the relative abundance of the Ge_nLi_m clusters, photoionized by an ArF laser, is subjected to a detailed theoretical investigation within the framework of the most popular density functional theory formalism. The periodic appearance of the peaks corresponding to $\text{Ge}_9\text{Li}_{4-5}$, $\text{Ge}_{18}\text{Li}_{5-7}$, $\text{Ge}_{27}\text{Li}_{9-12}$, $\text{Ge}_{36}\text{Li}_{13-16}$, and $\text{Ge}_{45}\text{Li}_{16-21}$ in the mass spectrum clearly suggests the existence of the Ge_9 building blocks, which is well-known for the group 14 elements. On the basis of our complementary theoretical investigation, we were able to propose a theoretical model which rationalizes the experimental spectrum. Our systematic theoretical investigation supports the fact that doping with lithium atoms enhances the stability of the Ge cluster, where the Li atom mainly acts as charge balancer. We report for the first time the presence of oligomers of $[\text{Ge}_9]^{x-}$ units in a gas-phase experiment.

1. Introduction

The discovery of fullerenes¹ and carbon nanotubes² triggered the birth of a very successful research area in physics and chemistry. This has led to several applications that are linked to already available technology. These include nanoelectronic devices, quantum wires, electron field emitters for ultrathin TV-screens, nanoprobes, high resolution tips for scanning and atomic force microscopes, sensors, ultra-high-strength composites, gas storage nanodevices, parts of nanomachines, etc. Today, by combining many of the unique electrical and mechanical properties of carbon nanotubes, scientists have devised a fully functional nanotube radio.³ Doping of fullerene, C_{60} , by alkali metal atoms is found to enhance its molecular hydrogen adsorption capacity.⁴ Nanotubes filled with biologically active molecules may be used as vehicles for drug delivery in living organisms.⁵

On the other hand, the study of homoatomic clusters of uniform size has opened up new avenues for the development of nanoscaled materials.⁶ Defined as nanometer sized entities built up from a few to many thousands of atoms, clusters comprise the middle between bulk materials and molecules. However, clusters cannot just be considered as small solid particles, since their properties are size-dependent in a nontrivial, nonscalable way. Among various polyhedra from group IV elements, nine-atom clusters received considerable attention,⁷ in particular since for these sizes cluster coupling phenomena are identified, showing controlled oligomer and polymer cluster growth patterns. Dimers, trimers, tetramers, and even infinite chains of Ge_9^{x-} were synthesized in solution by the Sevov group.⁸ Red crystals were obtained, from which X-ray diffraction revealed the alternated ‘up’ and ‘down’ stacking of *tricapped*

trigonal prism Ge_9 units. The reduction of the overall charge is not completely understood. Band structure calculations suggest delocalized bonding with a charge requirement of 2^- per Ge_9 unit for all polymeric doubly linked chains.⁹ The reactivity of Ge_9 is not limited to the formation of polymers. Ge_9^{4-} can for instance be functionalized by a variety of R groups such as SbPh_2 , SbPh_2 , BiPh_2 , GeMe_3 , GePh_3 , SnMe_3 , SnPh_3 , etc.¹⁰ Reactions in solution of K_4Ge_9 with $\text{Ni}(\text{COD})_2$ (COD = cyclooctadiene) and $\text{Ni}(\text{PPh}_3)_2$ resulted in Ni-ligand capped Ge_9 clusters, some with and some without the presence of an interstitial nickel atom.¹¹ The presence of an interstitial atom will alter the electronic structure of the cluster, making it possible to modulate the optical response. The doping with single dopants can be extended; a linear dimer is found to be present in $[\text{Ni}_3@(\text{Ge}_9)_2]^{4-}$ by enlarging the system to two vertex-fused Ge_9 clusters. This realization can be conceived as the onset of a magnetic nanorod.

In this context, we set out to investigate the formation of germanium clusters in the presence of lithium atoms. The wealth of experimental observations and the reported coupling schemes demanded a detailed theoretical investigation. The structural and energetic information of gas-phase clusters can mainly be approached via quantum chemical computations. We report here for the first time the formation of the $[\text{Ge}_9]^{x-}$ oligomers in a gas-phase experiment complemented by a detailed theoretical characterization.

The present article is organized in the following way. A brief overview of the experimental setup is discussed in the first part followed by the applied theoretical methodologies. Experimental results are presented in the next section along with a systematic computational analysis of lithium-doped germanium clusters, Ge_nLi_m ($n = 4, 5$; $m = 1, 2, 3$) and Ge_nLi_m ($n = 6-8$; $m = 1, 2$). The structural pattern of the higher members detected in the spectrum, namely, Ge_9Li_5 , $\text{Ge}_{18}\text{Li}_6$, $\text{Ge}_{27}\text{Li}_{11}$, and $\text{Ge}_{35}\text{Li}_{16}$, are resolved within a proposed theoretical model. We thus probe the nine-atom building blocks, the coupling pattern, and the role

* To whom correspondence should be addressed. E-mail: peter.lievens@fys.kuleuven.be; minh.nguyen@chem.kuleuven.be.

[†] Department of Chemistry and INPAC.

[‡] Laboratory of Solid State Physics and INPAC.

of Li atoms using our DFT calculations, which are reported in the respective sections.

2. Experimental Overview

Lithium-doped germanium clusters are produced using a dual-laser dual-target vaporization source.¹² Two rectangular targets of Ge and Li are placed beside each other and are moved in a closed-loop pattern under computer control. The targets are exposed to the focused 532 nm laser light of two pulsed Nd: YAG lasers. Synchronously with the ablation of the target surfaces, helium gas is injected into the source by a pulsed gas valve, typically with a pressure of 5 to 7 bar. Cluster formation is initiated by collisions between atoms, dimers, and trimers of the vaporized material and inert-gas atoms. The mixture of atoms, clusters, and inert gas undergoes a supersonic expansion into a vacuum chamber through a nozzle. The nozzle has a conical shape with an opening angle of 10° and a throat diameter of 1.2 mm. The isentropic expansion reduces the temperature of the cluster beam and because of the rapidly decreasing density, ends the cluster-growth process.

The clusters are detected by a reflectron time-of-flight (RTOF) mass spectrometer ($M/\Delta M \approx 800$). Both ionic and neutral clusters are produced. The cationic clusters (direct ions) are studied directly by the RTOF, while for neutral clusters, additional laser ionization is employed. Here the ionic clusters are eliminated from the beam by electrostatic deflection before entering the mass spectrometer. In the extraction region, neutral clusters are ionized by low fluence (250 $\mu\text{J}/\text{cm}^2$), high energy laser light (6.4 eV, ArF excimer laser).

3. Computational Methodologies

We have used the density functional theory formalism in conjunction with LANL2DZ, aug-cc-pVDZ-pp, Stuttgart RLC ECP, and SV(P) for the present analysis. For the study of the clusters ranging from Ge_4Li_m - Ge_5Li_m , the preliminary geometry optimizations are performed using a small LANL2DZ basis set and then reoptimizations are performed using the larger aug-cc-pVDZ-pp basis set where pp stands for a pseudopotential replacing the cores. The located stationary points are characterized as minima evaluating the vibrational frequencies at the same level. For the larger clusters ranging from Ge_9Li_m to $\text{Ge}_{36}\text{Li}_m$, geometry optimizations are performed with the Stuttgart relativistic large core (RLC) effective core potential (ECP) basis set implemented in the Turbomole suites of programs. An effective core potential for the 28 electrons of germanium and 2 electrons of lithium has been modeled using the aforementioned basis set. Parallel computations are also carried out with a TZV(P) basis set for the Ge_5Li_3 and were found in agreement with the ECP computations. The relevant minima are again reconfirmed using the SV(P) basis set which has the same quality as that of the 6-31G(d) basis set. All computations are performed with Gaussian 03 revision D02¹³ and Turbomole V5.8¹⁴ suites of programs. The optimized geometries are plotted with Molden,¹⁵ Gaussview,¹⁶ and gOpenmol¹⁷ and are reported in the respective sections.

4. Results and Discussion

(a) Experimental Results. Figure 1 shows a RTOF mass abundance spectrum of photoionized lithium-doped germanium clusters. The vertical lines match the position of pure germanium clusters. Only very small traces of pure germanium clusters are present. The spectrum is dominated by broad shapes, consisting of multiple peaks which reflect the coexistence of Ge_n clusters

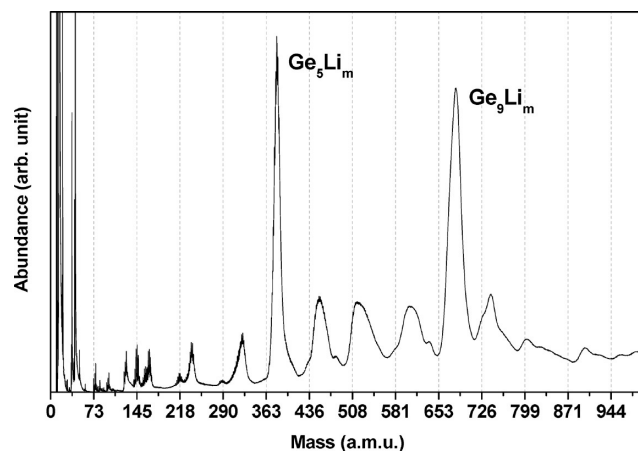


Figure 1. RTOF mass abundance spectrum of Ge_nLi_m clusters, photoionized by an ArF laser (6.4 eV, 250 $\mu\text{J}/\text{cm}^2$). The vertical lines match the position of pure Ge clusters.

doped with different amounts of Li. For each value of n there is an optimal stoichiometry between germanium and lithium atoms. Because of the isotopic nature of germanium and lithium, the contributing peaks cannot readily be resolved with our current instrumentation except for the smallest sizes. To determine the precise stoichiometry for the most abundant clusters, each conglomerate of peaks was fitted with the isotope pattern for the corresponding bare germanium cluster. The isotope patterns are taken from a reference spectrum at the same experimental conditions as the doped spectrum. This is illustrated in Figure 2, which shows the experimental and fitted mass peaks of Ge_4Li_m as well as contributions of Ge_4 , Ge_4Li_3 , Ge_4Li_4 , and Ge_4Li_5 .

While for Ge_4Li_m a small trace of the bare germanium cluster is still visible in the mass spectrum, this is generally not the case. The lack of clear reference peaks and the small mass of the lithium atom makes the mass calibration vulnerable to human bias. To address this problem, a range of spectra with different amounts of lithium in the cluster production were plotted against each other. This picture reveals a clear transition, where doped germanium peaks grow at the expense of the bare germanium peaks. With the bare germanium spectrum as a reference, the error on the mass calibration for all spectra stays below 3 amu for sizes below Ge_{10} , making assignment of each peak in this mass range unambiguous.

Table 1 summarizes the abundances for Ge_nLi_m for $n = 1$ to 10, relative to the most abundant doped cluster for each size. For the smallest Ge_nLi_m clusters, a low abundance of doped clusters is found and bare germanium peaks are still present. For the lithium-doped germanium monomer, one to three Li atoms are found, but all species are heavily oxidized. GeLi_3O_2 turns out to be the most abundant, with no apparent unoxidized GeLi_3 in the mass spectrum, closely followed by GeLi(O) . Smaller peaks are found for $\text{GeLi}_2(\text{O})$. For the dimer and trimer, Ge_2Li_m and Ge_3Li_m show comparable behavior with small amount of lithium doping and a maximum for $m = 3$. In both cases, traces of oxidized species are insignificantly low. For Ge_4Li_m the maximal amount of doping has shifted to $m = 5$, with a smaller contribution for $m = 4$ also present.

The size range from $n = 5$ to 10 shows high abundances of several doped germanium clusters. Most distinct are the sizes $n = 5$ and $n = 9$. Ge_5Li_m has a sharp peak at $m = 3$ and a small tail. Although this peak is very high, the bare Ge_5 peak is almost absent, both in the doped and bare germanium mass spectra. For Ge_6Li_m there is a strong peak with a long tail at $m = 2$,

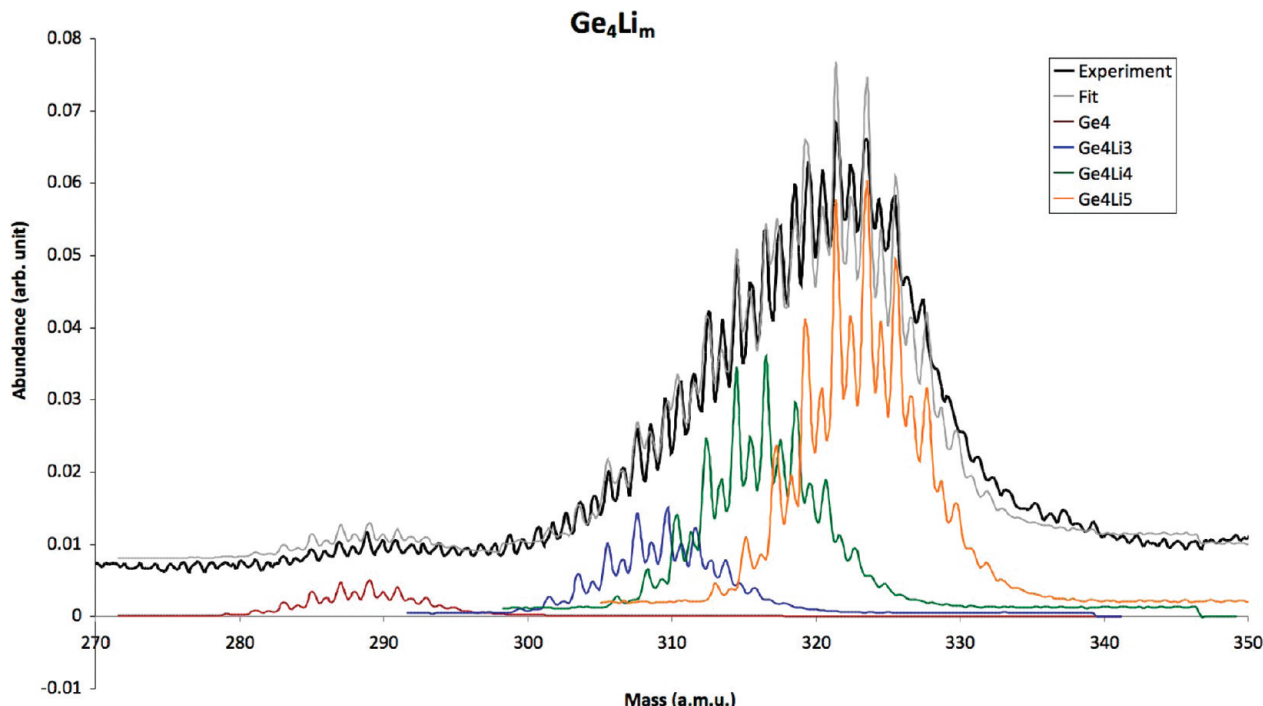


Figure 2. The mass spectrum around Ge_4Li_m (black) is fitted (light gray) by the isotope pattern from a pure Ge reference spectrum. Significant contributions are found present for Ge_4Li_0 , Ge_4Li_3 , Ge_4Li_4 , and Ge_4Li_5 . (A color version of this figure is available online.)

TABLE 1: Relative Abundances of Ge_nLi_m Clusters for Different Values of n Ranging from 1 to 10^a

Ge ₁ Li ₁ (0.4), Li ₁ O (0.6), Li₃O₂ (1)
Ge ₂ Li ₂ (0.6), Li₃ (1)
Ge ₃ Li₃ (1)
Ge ₄ Li ₄ (0.6), Li₅ (1)
Ge ₅ Li₃ (1)
Ge ₆ Li ₂ (1), Li ₃ (0.5), Li ₄ (0.5)
Ge ₇ Li₁ (1) , Li ₂ (0.5), Li ₃ (0.5), Li ₄ (0.4)
Ge ₈ Li ₁ (0.5), Li ₂ (0.6), Li₃ (1) , Li ₄ (0.6), Li ₅ (0.7), Li ₈ (0.3)
Ge ₉ Li ₃ (0.7), Li ₄ (0.9), Li₅ (1)
Ge ₁₀ Li₂ (1) , Li ₃ (0.8)

^a The most abundant species for each germanium cluster size are indicated in bold and are assigned an arbitrary value of 1. Only clusters with relative abundances higher than 0.2 are included in this list.

while for Ge_7Li_m the envelope peak starts at $m = 1$. It is unlikely, but not excluded, that part of the tail is due to oxidized species. Ge_5Li_3 , Ge_6Li_2 , and Ge_7Li_1 each have eight atoms. The situation for Ge_8Li_m is less straightforward; though there is a maximum for $m = 3$, a broad size range of lithium atoms leads to competing structures. While for bare germanium clusters, Ge_{10} is more abundant than Ge_9 , upon doping this order is reversed. Ge_9Li_m is centered around Ge_9Li_4 , but Ge_9Li_3 and Ge_9Li_5 are also clearly present, as the peak is significantly broader than the bare Ge_9 peak. Ge_8Li_5 is most abundant, closely followed by Ge_8Li_4 . $\text{Ge}_{10}\text{Li}_m$ has a maximum for $m = 2$ but noticeably also has a significant contribution from the bare germanium peak. Ge_{11} and Ge_{12} do not gain much intensity upon doping and remain small as in the bare mass spectrum.

Though the larger clusters are less abundant than the smaller ones, a periodic appearance of peaks at larger scale is striking. Figure 3 shows a mass spectrum resulting from a photoionization process at low laser fluence. The dotted vertical lines are plotted at the positions that match the abundances of Ge_{9p} ($p = 1-5$) clusters. The peaks in this part of the mass spectrum also are broadened because of the natural isotope distribution for

germanium and the coexistence of different amounts of lithium doping. The first peak in this pattern is Ge_9Li_m . The central position of the other enhanced peaks can be estimated from the mass spectra as corresponding to $\text{Ge}_{18}\text{Li}_{5-7}$, $\text{Ge}_{27}\text{Li}_{9-12}$, $\text{Ge}_{36}\text{Li}_{13-16}$, and $\text{Ge}_{45}\text{Li}_{16-21}$. The absence of clear reference peaks makes precise determination of the stoichiometry of the larger clusters impossible with our instruments' current mass resolution; hence, the number of lithium atoms is given by a range instead of a precise number. The observation that the mass interval between these clusters equals Ge_9 is very interesting since nine-atom anions from group IVa elements are discovered to behave like building blocks in many chemical experiments.⁷⁻¹¹

(b) Computational Results. The structural probe of the aforementioned mass spectrum demands a thorough computational investigation. With this goal in mind we have performed a systematic analysis on the geometries to find the building pattern of these clusters. It is obvious that practical difficulties in locating the global minimum increase with increasing cluster size. It has been demonstrated that the traditional Monte Carlo and molecular dynamics simulated annealing approaches often encounter difficulties finding the global minima for particular types of interatomic interactions.¹⁸ There exists no universal methodology for locating the global minimum, while popular approaches include genetic algorithms¹⁹ and stochastic search methods.^{20,21} In the present contribution we have adopted extensive geometry optimization methodologies on various estimated structures for the lower members of the lithium-doped clusters while a theoretical model has been proposed and validated at the end for larger members of the series seen in the mass spectrum. As is seen in Table 1 the most abundant species for Ge_nLi_m with $n = 2$ and 3 are Ge_2Li_3 and Ge_3Li_3 . These clusters were subjected to extensive theoretical studies using the robust *ab initio* methodologies and the popular density functional approach recently.^{22,23} Structurally Ge_2Li_3 falls under C_{2v} symmetry and an electronic state of ${}^2\text{A}_2$ has been derived, while a C_s symmetric ${}^2\text{A}'$ has been located as the global minimum for Ge_3Li_3 .^{22,23} In the present article we have carried

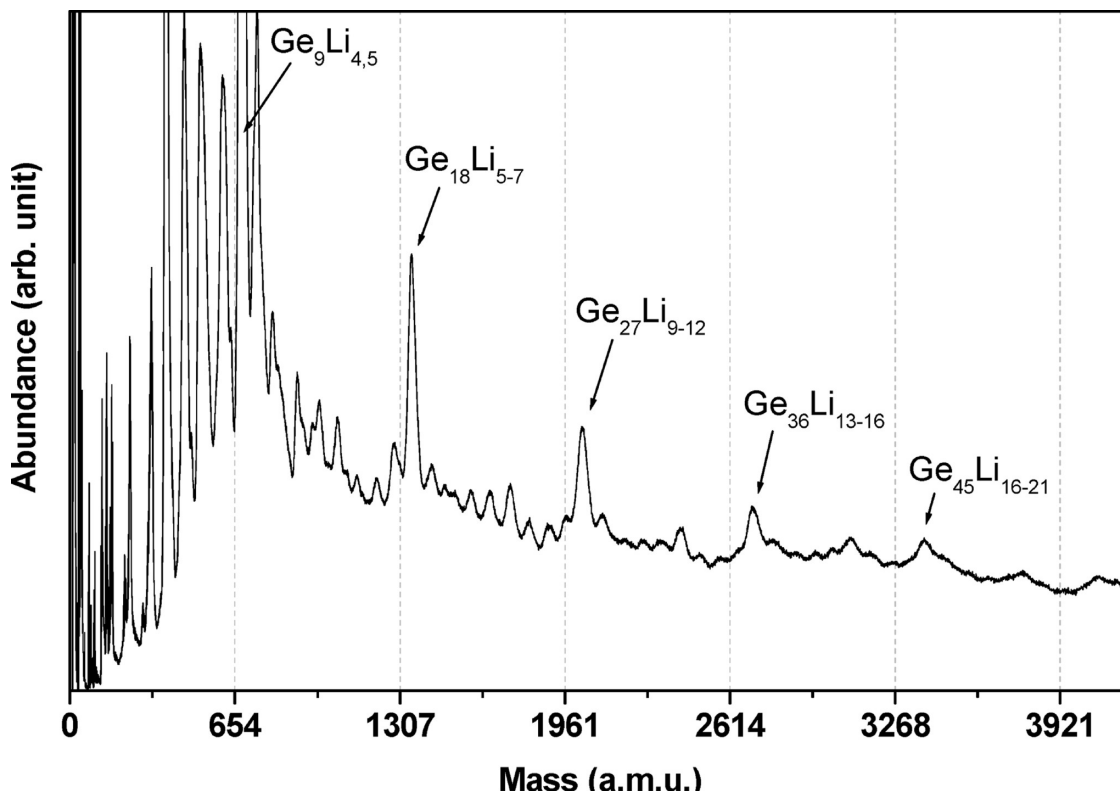


Figure 3. RTOF mass abundance spectrum of Ge_nLi_m clusters photoionized by ArF laser light (6.4 eV, $250 \mu\text{J}/\text{cm}^2$). The vertical lines match the position of pure Ge_9 clusters.

out a systematic analysis on Ge_nLi_m ($n = 4, 5; m = 1, 2, 3$) and Ge_nLi_m ($n = 6, 7, 8; m = 1, 2$), which are reported in the following sections.

(i) Ge_nLi_m ($n = 4, 5; m = 1, 2, 3$). As the first step toward an analysis of lithium-doped Ge_4 we have reinvestigated the electronic structure of Ge_4 systems. The most recent studies were reported by Xu et al.²⁴ where they examined a series of Ge_n structures. On the basis of density functional computations in conjunction with a double- ζ basis set, a rhombic structure was located for the tetramer. Our results in conjunction with a large aug-cc-pVDZ-pp basis set are in agreement with this finding. The located global minimum falls under the D_{2h} symmetry, and an electronic state ${}^1\text{A}_g$ has been derived. Molecular geometries for the lowest-lying neutral and anionic Ge_4 system along with selected geometrical parameters are reported in Figure 4, and the total and relative energies are listed in Table 2. Note that the $\text{Ge}-\text{Ge}$ bond length is 2.483 Å and the two different bond angles are 116.0° and 64.0°. In the triplet manifold we located a C_{2v} rhombic structure with a singlet-triplet energy gap of 21.6 kcal/mol at the DFT level. The geometrical change from singlet to triplet includes the shortening of the $\text{Ge}-\text{Ge}$ bond and increase in the $\text{Ge}-\text{Ge}-\text{Ge}$ bond angle by ~5°.

Addition of an electron leads to the formation of the anion for which a rhombic lowest-lying structure has been located similar to the neutral molecule. On the basis of our DFT computations, an electronic state of ${}^2\text{B}_{2g}$ has been derived and is in agreement with the previously reported structure.²⁴ Geometrically this structure is very much similar to the neutral counterpart. The geometrical changes are marginal, with increase in the $\text{Ge}-\text{Ge}$ bond length by 0.01° and bond angle by 2°. In the quartet manifold we were able to locate a lowest-lying butterfly-like structure, which falls under the C_{2v} point group symmetry along with an electronic state ${}^4\text{A}_2$. The doublet-quartet energy gap has been estimated to be ~40 kcal/mol at the B3LYP/aug-cc-pVDZ-pp level in favor of the low-spin state.

Doping with lithium atoms changes the electronic structure of the tetramer considerably. To investigate the structural changes, we have adopted a progressive doping methodology. The located lowest-lying structures corresponding to the mono-, di-, and trilithiated neutral tetramers are illustrated in Figure 4, and the ones corresponding to the cationic tetramers are given in Figure 5. Some selected geometrical parameters also are reported in the respective figures. For a complete analysis, we have performed our geometry optimizations in both spin manifolds, and the results are included in Figure 4 and Figure 5 for comparison.

The total and relative energies of the located minima are listed in Table 3. It is clear that the first lithium prefers a bridging position to the rhombic germanium tetramer, in both spin manifolds. During the progressive doping, the Ge_4 unit undergoes a geometrical change from planar rhombic to a butterfly-like structure. Both neutral and cationic counter parts of the trilithiated germanium tetramer are geometrically similar in shape, while the $\text{Ge}-\text{Ge}$ and $\text{Ge}-\text{Li}$ bond lengths are shorter in the former. For all lithium-doped tetramers, we have managed to locate low-spin ground states. For monolithiated species, a doublet-quartet energy gap of 17.4 kcal/mol has been estimated, while the corresponding singlet-triplet gap of the dilithiated tetramer is 9.3 kcal/mol. For the trilithiated derivative, our DFT computations predict a larger doublet-quartet gap of 21.4 kcal/mol in favor of the low-spin state.

Xu et al.²⁴ reported a D_{3h} symmetric structure as the global minimum for the bare neutral Ge_5 . Our DFT analyses concur with the aforementioned study predicting a singlet D_{3h} symmetric global minimum with a singlet-triplet energy gap of 17 kcal/mol at B3LYP/aug-cc-pVDZ-pp level. The total energy values of the lowest-lying structures are listed in Table 2, and their geometries are illustrated in Figure 6. In the case of the global minimum the $\text{Ge}-\text{Ge}$ bond lengths amount to 2.48 Å. We were also able to locate the lowest-lying ${}^3\text{B}_1$ triplet state,

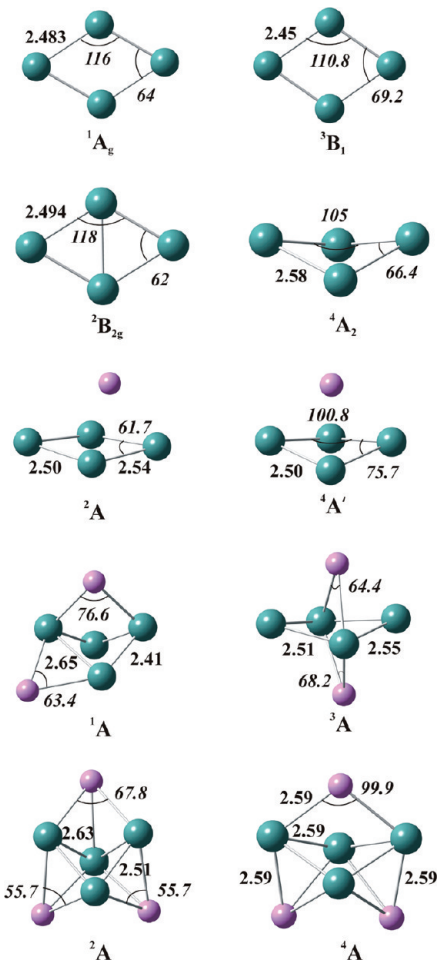


Figure 4. Molecular geometries for Ge_4 , Ge_4^- , and Ge_4Li_m ($m = 1, 2, 3$) in its lowest-lying electronic states, optimized at B3LYP/aug-cc-pVDZ-pp. Dark slate gray balls are germanium and deep pink balls are lithium atoms. Bond lengths are given in angstroms and bond angles in degrees.

TABLE 2: Total and Relative Energies of Ge_n ($n = 4-5$) at B3LYP/aug-cc-pVDZ-pp Level

molecule	state	total (hartree) and relative energies (kcal/mol in parentheses) at B3LYP/aug-cc-pVDZ-pp ^a		relative energy kcal/mol eV	
		(total energy values are in hartrees)			
Ge_4	$^1\text{A}_g$	-1178.627627	0	0	0
	$^3\text{B}_1$	-1178.593161	21.63	0.94	
Ge_4^-	$^2\text{B}_{2g}$	-1178.695902	0	0	
	$^4\text{A}_2$	-1178.631983	40.11	1.74	
Ge_5	$^1\text{A}'$	-1473.308289	0	0	
	$^3\text{B}_1$	-1473.281212	16.99	0.74	
Ge_5^-	$^2\text{A}''$	-1473.385589	0	0	
	^4A	-1473.341104	27.91	1.21	

^a The total energies are scaled with ZPE computed at the same level.

energetically lying 17 kcal/mol above the singlet ground state. The triplet state falls under C_{2v} symmetry, and there is considerable change in geometry following the singlet-triplet excitation. Addition of an electron results in the formation of an anion, for which a doublet ground state $^2\text{A}''$ has been characterized. The lowest-lying quartet state has been derived which lies at 28 kcal/mol above the low-spin state. Selected geometrical parameters of the corresponding structures are given in Figure 6.

Doping of the Ge_5 unit with lithium atoms shows the same trend as in the case of the tetramer where the latter normally

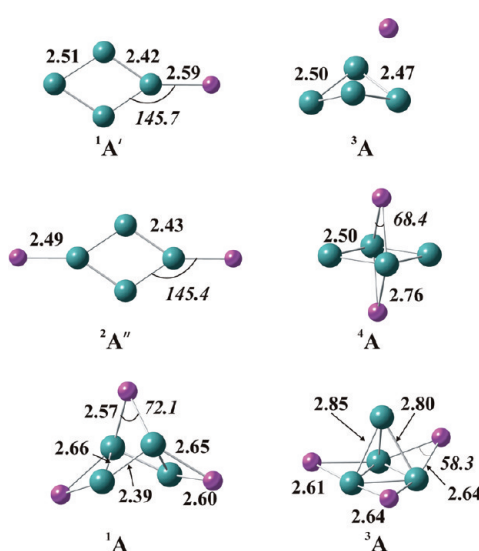


Figure 5. Molecular geometries for Ge_4Li_m^+ ($m = 1, 2, 3$) in its lowest-lying electronic states, optimized at B3LYP/aug-cc-pVDZ-pp. Dark slate gray balls are germanium and deep pink balls are lithium atoms. Bond lengths are given in angstroms and bond angles in degrees.

TABLE 3: Total and Relative Energies of Ge_4Li_m ($m = 1-3$) at B3LYP/aug-cc-pVDZ-pp Level

molecule	state	total (hartree) and relative energies (kcal/mol in parentheses) at B3LYP/aug-cc-pVDZ-pp ^a		relative energy kcal/mol eV	
		(total energy values are in hartrees)			
Ge_4Li	^2A	-1186.172891	0	0	0
	$^4\text{A}'$	-1186.145181	17.39	0.75	
Ge_4Li^+	$^1\text{A}'$	-1185.958705	0	0	
	^3A	-1185.924309	21.58	0.94	
Ge_4Li_2	^1A	-1193.735186	0	0	
	^3A	-1193.720416	9.27	0.40	
$\text{Ge}_4\text{Li}_{2+}$	$^2\text{A}''$	-1193.521784	0	0	
	^4A	-1193.49093	19.36	0.84	
Ge_4Li_3	^2A	-1201.295769	0	0	
	^4A	-1201.26162	21.43	0.93	
Ge_4Li_3^+	^1A	-1201.103499	0	0	
	^3A	-1201.082941	12.9	0.56	

^a The total energy values are scaled with ZPE computed at the same level.

acts as a bridging entity. In the case of the neutral system, progressive lithiation occurs at successive positions leading to the C_{2v} symmetric trilithiated Ge_5 . The located global minima for mono-, di-, and trilithiated neutral Ge_5 are illustrated in Figure 6 along with their high-spin counterparts. Total and relative energies are listed in Table 4. Upon the singlet-triplet excitation, the geometrical change is invariably significant, leading to large distortions of the Ge_5 unit. At this moment it is important to discuss the structure of Ge_5Li_3 , as the mass spectrum (Figure 3) shows an increased abundance of that cluster. On the basis of the present analysis, we were able to derive a C_{2v} structure for Ge_5Li_3 . This structure can better be modeled as derived from the triplet $^3\text{B}_1$ state of the neutral Ge_5 . The three lithium atoms mainly act as the bridging units with three different $\text{Ge}-\text{Li}$ bond distances of 2.64, 2.53, and 2.57 Å. The $\text{Ge}-\text{Ge}$ bond length amounts to 2.6 Å. During the doublet-quartet excitation, considerable change in the geometry occurs, mainly the Ge_5 unit undergoing strong distortion. Structurally, the cationic structures take different geometries as compared to the neutral counterpart. Optimized shapes of mono-, di-, and trilithiated cationic Ge_5 clusters are illustrated in Figure 7 along with their selected geometrical parameters. For the

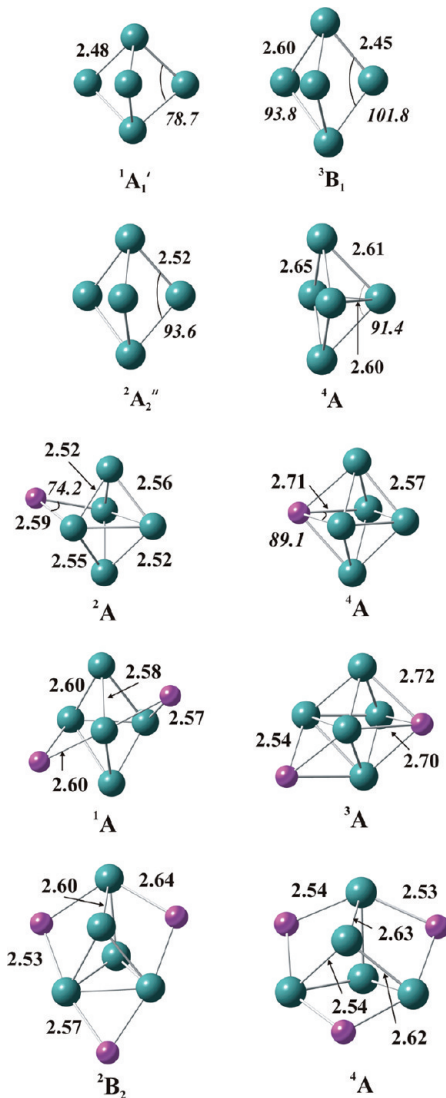


Figure 6. Molecular geometries for Ge₅, Ge₅⁻, and Ge₅Li_m ($m = 1, 2, 3$) in its lowest-lying electronic states, optimized at B3LYP/aug-cc-pVDZ-pp. Bond lengths are given in angstrom units and bond angles in degrees.

TABLE 4: Total and Relative Energies of Ge₅Li_m ($m = 1-3$) at B3LYP/aug-cc-pVDZ-pp Level

molecule	state	total and relative energies (in parentheses) at B3LYP/aug-cc-pVDZ-pp level ^a	relative energy	
			kcal/mol	eV
Ge ₅ Li	² A	-1480.868601	0	0
	⁴ A	-1480.824464	27.7	1.2
Ge ₅ Li ⁺	¹ A	-1480.640536	0	0
	³ A	-1480.614365	16.42	0.71
Ge ₅ Li ₂	¹ A	-1488.444612	0	0
	³ A	-1488.415502	18.27	0.79
Ge ₅ Li ₂ ⁺	² A	-1488.219331	0	0
	⁴ A	-1488.167982	32.22	1.40
Ge ₅ Li ₃	² A	-1495.981919	0	0
	⁴ A	-1495.949101	20.59	0.89
Ge ₅ Li ₃ ⁺	¹ A	-1495.811099	0	0
	³ A	-1495.776943	21.43	0.93

^a The total energy values are scaled with ZPE computed at the same level.

lithium-doped Ge₅ clusters, our present analysis consistently suggested a low-spin ground state.

(ii) Ge_nLi_m ($n = 6, 7, 8$; $m = 1, 2$). We have carried out the same procedure to characterize the structure of the lowest-lying

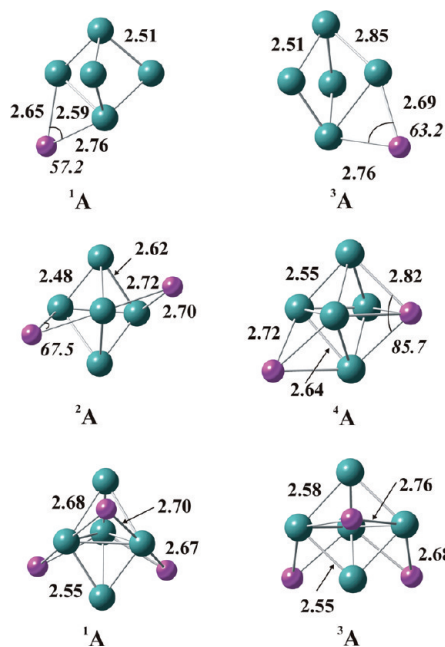


Figure 7. Molecular geometries for Ge₆Li_m⁺ ($m = 1, 2, 3$) in its lowest-lying electronic states, optimized at B3LYP/aug-cc-pVDZ-pp. Dark slate gray balls are germanium, and deep pink balls are lithium atoms. Bond lengths are given in angstrom units and bond angles in degrees.

isomers of lithium-doped germanium clusters with number of germanium atoms ranging from 6 to 8. As the number of isomers increases with the cluster size, locating the global minimum is extremely difficult in the case of larger clusters. However, on the basis of our extensive geometry optimizations on various estimated structures, we were able to derive a singlet ¹A₁ electronic state as the global minimum for Ge₆. There were no experimental geometries available for both Ge₆, and its anion and our result is consistent with the one reported previously.²⁴ A singlet-triplet (¹A₁ ~ ³A₂) energy gap of 16 kcal/mol has been estimated at B3LYP/aug-cc-pVDZ-pp level. Optimized geometries of the lowest-lying electronic states of Ge₆ and its cation and anion are illustrated in Figure 8 whereas the total and relative energies are given in Table 5. The singlet-triplet transition accompanies a geometric change resulting in the shortening of the outer Ge–Ge bond by an amount of 0.2 Å; important geometrical parameters also are given in the respective figures. Removal of an electron resulted in the formation of the cation for which our DFT analysis derived a *C*_{2v} symmetric ²B₁ lowest-lying electronic state. In the case of the Ge₆⁻ anion, in agreement with the previous theoretical computations, we have found the lowest-lying ²A_{2u} state.

In the case of Ge₇ a *D*_{5h} symmetric ¹A₁' electronic state has been located as the global minimum in the potential energy surface (cf. Figure 8). A lower-lying triplet state, ³B₁, similar in shape to the ground electronic state has also been derived with a singlet triplet energy gap of 27 kcal/mol at B3LYP/aug-cc-pVDZ-pp level. Our computations derived low-spin electronic states for the ions; a *C*_{2v} symmetric cation, ²A₁, and a *D*_{5h} symmetric anion, ²A₂. Optimized geometries and selected geometrical parameters are illustrated in Figure 8, and the total and relative energies are given in Table 5. For Ge₈ a *C*_s symmetric ¹A' ground state has been located, with a low-lying *C*_{2v} symmetric triplet ³B₂ state. The singlet triplet energy gap is estimated to be 17 kcal/mol at B3LYP/aug-cc-pVDZ-pp level. The located low-lying electronic states of cation and anion are illustrated in Figure 8 along with the neutral counterpart.

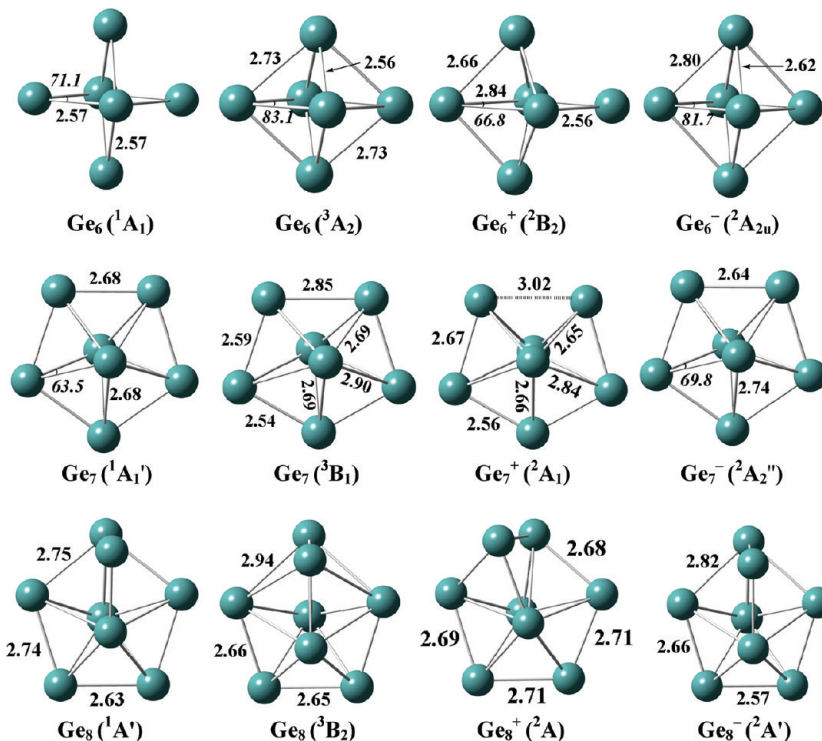


Figure 8. Molecular geometries for Ge_n , Ge_n^+ , and Ge_n^- ($n = 6, 7, 8$) in its lowest-lying electronic states, optimized at B3LYP/aug-cc-pVDZ-pp. Bond lengths are given in angstroms and bond angles in degrees.

TABLE 5: Total and Relative Energies of $\text{Ge}_n^{0,+1,-1}$ ($n = 6, 7, 8$) Obtained at B3LYP Level Using aug-cc-pVDZ-pp Basis Set^a

molecule	state	total energy (a.u.)	relative energy	
			kcal/mol	eV
Ge_6	${}^1\text{A}_1$	-1767.99858	0.0	0.0
	${}^3\text{A}_2$	-1767.97302	16.0	0.7
Ge_6^+	${}^2\text{B}_2$	-1767.73214	167.2	7.3
Ge_6^-	${}^2\text{A}_{2u}$	-1768.06824	-43.7	-1.9
Ge_7	${}^1\text{A}'_1$	-2062.68804	0.0	0.0
	${}^3\text{B}_1$	-2062.64504	27.0	1.2
Ge_7^+	${}^2\text{A}_1$	-2062.41760	169.7	7.4
Ge_7^-	${}^2\text{A}_2''$	-2062.75837	-44.1	-1.9
Ge_8	${}^1\text{A}'$	-2357.33289	0.0	0.0
	${}^3\text{B}_2$	-2357.30602	16.9	0.7
Ge_8^+	${}^2\text{A}$	-2357.08811	153.6	6.7
Ge_8^-	${}^2\text{A}'$	-2357.41141	-49.3	-2.1

^a The total energy values are scaled with ZPE at the same level.

Upon doping with lithium atoms, the geometries and electronic structure of bare germanium clusters changes considerably. Optimized geometries for the mono- and dilithiated Ge_6 and their cations are illustrated in Figure 9 along with selected geometrical parameters. The total and relative energies of lithium-doped germanium clusters with the number of germanium atoms ranging from 6 to 8 are listed in Table 6. For Ge_6Li a doublet ${}^2\text{B}_2$ electronic state has been derived under C_{2v} symmetry which is geometrically similar to the lowest-lying electronic state of Ge_7 . A lowest-lying quartet state ${}^4\text{A}''$ also has been derived under C_s symmetry with a doublet quartet energy gap of 25 kcal/mol at B3LYP/aug-cc-pVDZ-pp level. The geometries of the cations are considerably different from that of the neutral counterparts for which a singlet ${}^1\text{A}_1$ low-lying state has been derived with a singlet triplet energy gap of 20 kcal/mol. Progressive lithiation results in Ge_6Li_2 with a C_s symmetric ${}^1\text{A}'$ electronic state. The structure can be better modeled as two lithium atoms distributed symmetrically around

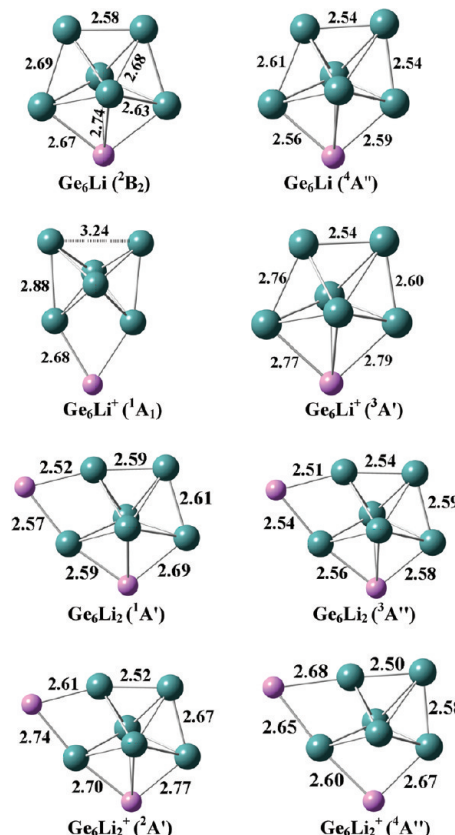


Figure 9. Molecular geometries for $\text{Ge}_6\text{Li}_m^{0,+1}$ ($m = 1, 2$) in its lowest-lying electronic states, optimized at B3LYP/aug-cc-pVDZ-pp. Dark slate gray balls are germanium, and deep pink balls are lithium atoms. Bond lengths are given in angstroms and bond angles in degrees.

the Ge_6 unit. The geometry of the lowest-lying electronic state of the cation is very much similar to that of the neutral counterpart (cf. Figure 9).

TABLE 6: Total and Relative Energies of $\text{Ge}_n\text{Li}_m^{0,+1}$ ($n = 6, 7, 8, m = 1, 2$) obtained at B3LYP Level Using aug-cc-pVDZ-pp Basis Set^a

molecule	state	total energy (a.u.)	relative energy	
			kcal/mol	eV
Ge_6Li	$^2\text{B}_2$	-1775.54938	0.0	0.0
	$^4\text{A}''$	-1775.50938	25.1	1.1
Ge_6Li^+	$^1\text{A}_1$	-1775.33008	0.0	0.0
	$^3\text{A}'$	-1775.29694	20.8	0.9
Ge_6Li_2	$^1\text{A}'$	-1783.11427	0.0	0.0
	$^3\text{A}''$	-1783.08249	19.9	0.9
Ge_6Li_2^+	$^2\text{A}'$	-1782.89804	0.0	0.0
	$^4\text{A}''$	-1782.85675	25.9	1.1
Ge_7Li	$^2\text{B}_1$	-2070.23024	0.0	0.0
	$^4\text{A}''$	-2070.17286	36.0	1.6
Ge_7Li^+	$^1\text{A}_1$	-2070.02765	0.0	0.0
	$^3\text{B}_1$	-2069.98392	27.4	1.2
Ge_7Li_2	$^1\text{A}_1$	-2077.78175	0.0	0.0
	$^3\text{A}'$	-2077.74055	25.9	1.1
Ge_7Li_2^+	$^2\text{B}_1$	-2077.58685	0.0	0.0
	$^4\text{A}''$	-2077.52301	40.1	1.7
Ge_8Li	$^2\text{A}''$	-2364.88668	0.0	0.0
	$^4\text{A}''$	-2364.84837	24.0	1.0
Ge_8Li^+	$^1\text{A}'$	-2364.66177	0.0	0.0
	$^3\text{A}''$	-2364.65704	3.0	0.1

^a The total energy values are scaled with ZPE at the same level.

Optimized geometries of mono- and dilithiated Ge_7 are given in Figure 10 along with that of their cations. For Ge_7Li a C_{2v} symmetric $^2\text{B}_1$ state has been located in the potential energy surface as the global minimum. This structure can be better modeled as the Ge_7 unit with the lithium atom acting as a bridging entity. The geometry of the cation is similar to that of the neutral counterpart, while for the former a singlet low-lying electronic state $^1\text{A}_1$ has been derived under C_{2v} symmetry. Similar to the case of Ge_6Li_2 the progressive addition of the lithium atom to Ge_7Li prefers a symmetrical position around the Ge_7 unit. A lowest-lying singlet, $^1\text{A}_1$, electronic state has been derived for the same C_{2v} symmetry. The geometry of the low-lying isomer of the cation is similar to that of the neutral counterpart. At quartet manifold the geometries show considerable difference compared to that of the low-spin states. For Ge_8Li a C_s symmetric $^2\text{A}''$ electronic state has been derived based on our DFT computations with a doublet quartet gap amounting to 24 kcal/mol at B3LYP/aug-cc-pVDZ-pp level. The optimized geometries of Ge_8Li_m ($m = 1, 2$) along with that of the respective cations are illustrated in Figure 11, while the total and relative energies are given in Table 6. The geometries of the cations show considerable difference compared to the neutral species, for the former a singlet state, $^1\text{A}'$ within the C_s symmetry. Progressive addition of lithium leads to the formation of Ge_8Li_2 for which a singlet, $^1\text{A}'$, state has been derived based on our DFT computations. A singlet-triplet energy gap of 27 kcal/mol has been estimated at B3LYP/aug-cc-pVDZ-pp level. It can be seen that the geometries of the cations show considerable difference compared to that of the neutral counterparts.

(iii) **Ge_9Li_5 , $\text{Ge}_{10}\text{Li}_6$, $\text{Ge}_2\text{Li}_{11}$, and $\text{Ge}_3\text{Li}_{16}$.** Having carefully examined the geometrical and energetic properties of small Ge_nLi_m clusters, we are in a position to discuss the larger entities in order to probe the origin of the enhanced abundance of the periodic series of peaks in the experimental mass spectra. Significant progress in synthesis and characterization of nine-atom clusters of germanium has been made in recent years.⁷ One of the most noticeable recent discoveries is that clusters can couple to form polymers, providing hope to use $[\text{Ge}_9]^{x-}$ as a nanosize building block, hereby combining interesting chemi-

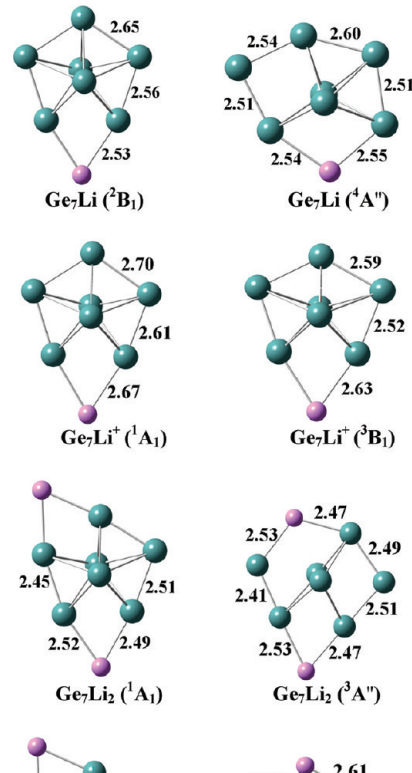


Figure 10. Molecular geometries for $\text{Ge}_7\text{Li}_m^{0,+1}$ ($m = 1, 2$) in its lowest-lying electronic states, optimized at B3LYP/aug-cc-pVDZ-pp. Dark slate gray balls are germanium, and deep pink balls are lithium atoms. Bond lengths are given in angstroms and bond angles in degrees.

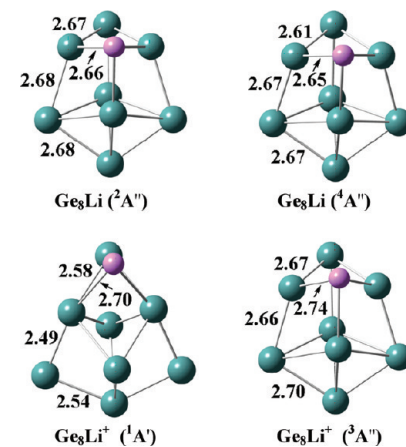


Figure 11. Molecular geometries for $\text{Ge}_8\text{Li}_m^{0,+1}$ ($m = 1, 2$) in its lowest-lying electronic states, optimized at B3LYP/aug-cc-pVDZ-pp. Dark slate gray balls are germanium, and deep pink balls are lithium atoms. Bond lengths are given in angstroms and bond angles in degrees.

cal and physical properties. Insertion of transition metal atoms might alter or improve the magnetic and optical properties of the single unit, while addition of organometallic fragments would envisage their application in chemical and biochemical nanomaterials. Here the identification of nine-atom building blocks, their coupling pattern, and the role of the Li atoms has been probed by our DFT calculations.

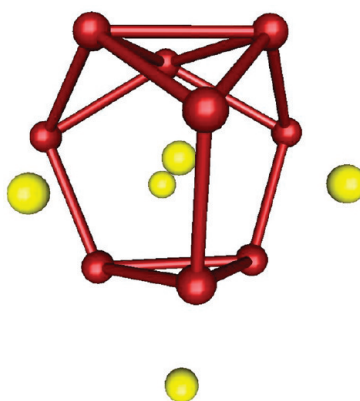


Figure 12. Optimized molecular geometry for Ge_9Li_5 at B3LYP/SV(P) level. Maroon color balls are germanium atoms, and yellow balls are lithium atoms.

TABLE 7: Total Energies of Different Structures Considered in the Proposed Theoretical Model at B3LYP/ECP^a and B3LYP/SV(P) Level

molecule	symmetry	total energies in hartrees scaled with ZPE computed at the same level	
		B3LYP/ECP ^a	B3LYP/SV(P)
Ge_9Li_5	C_s	-35.71192	-18727.82971
$\text{Ge}_{18}\text{Li}_6$	C_s	-70.48913	-37425.63569
$\text{Ge}_{27}\text{Li}_{11}$	C_{2v}	-106.24948	-56153.56307 ^b
$\text{Ge}_{36}\text{Li}_{16}$	C_s	-142.10538 ^b	-74881.51553 ^b

^a ECP basis set corresponds to Stuttgart RLC ECP. ^b Values are not scaled with ZPE.

TABLE 8: HOMO-LUMO Energy Gap in eV for Different Molecules Considered at B3LYP/ECP^a and B3LYP/SV(P) Level

molecule	HOMO–LUMO gap in eV	
	B3LYP/ECP ^a	B3LYP/SV(P)
Ge_9Li_5	1.21	1.20
$\text{Ge}_{18}\text{Li}_6$	2.68	2.96
$\text{Ge}_{27}\text{Li}_{11}$	0.27	0.17
$\text{Ge}_{36}\text{Li}_{16}$	1.76	1.87

^a ECP basis set corresponds to Stuttgart RLC ECP.

The geometry optimizations were performed for a large number of lithium-doped Ge_9 clusters. It was clear from the experimental analysis that the largest contribution toward the mass spectrum comes from $\text{Ge}_9\text{Li}_{4-5}$ clusters. On the basis of our extensive geometry search, we were able to derive a C_s symmetric structure as the global minimum of Ge_9Li_5 . This structure is a closed-cage structure with three fused pentagonal rings as displayed in Figure 12. Three lithium atoms serve as the bridging unit to the fused pentagonal rings, one lithium bridges the trigonal Ge_3 unit at the base, and one lithium atom is encapsulated in the cage. Total energies are listed in Table 7, and the HOMO–LUMO gap is included in Table 8. Several selected low-lying isomers and their relative energies with respect to the global minimum are illustrated in Figure 1S of Supporting Information.

Because of the expected existence of a large amount of structural isomers, we were not able to carry out a comprehensive structural analysis of the higher members of the series. However, we here propose a theoretical model toward a structural understanding of the larger clusters which is based on the formation of nine-atom clusters and their assembling. The available mass spectra data clearly represent a growth

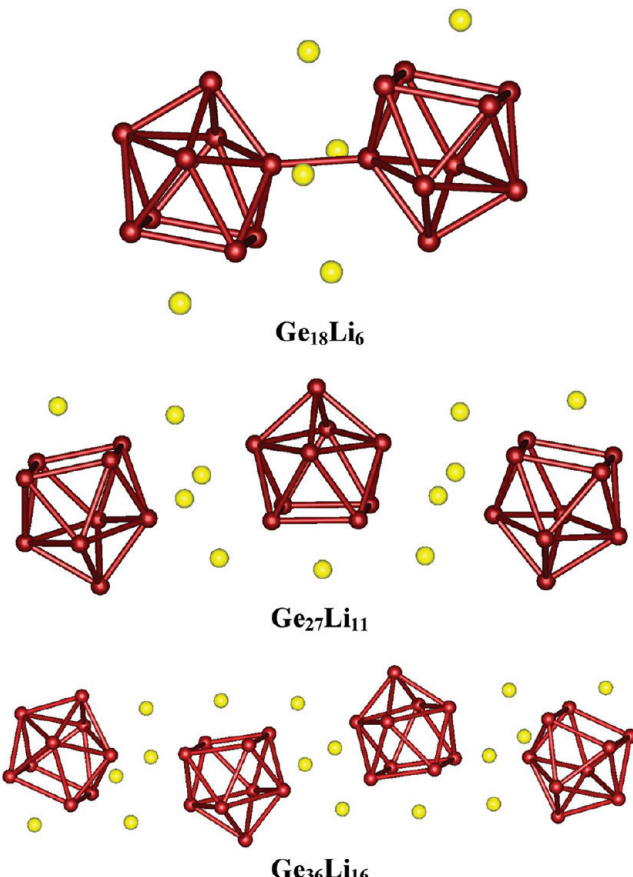


Figure 13. Optimized molecular geometry for $\text{Ge}_{18}\text{Li}_6$, $\text{Ge}_{27}\text{Li}_{11}$, and $\text{Ge}_{36}\text{Li}_{16}$ at B3LYP/SV(P) level within the proposed theoretical model. Maroon balls are germanium atoms, and yellow balls are lithium atoms.

pattern with Ge_9 units as building blocks. Structural details of a Ge_9 dimer, trimer, and tetramer have been characterized by the Sevov group⁸ as a combination of two *nido*- Ge_9 clusters, and a combination of three and four tricapped trigonal prisms arranged in a linear fashion. Of the various combinations considered, our computations suggest the combination of *nido*- Ge_9 units with several numbers of surrounding lithium atoms as the lowest energy ones. It is found that addition of successive Ge_9 units in a symmetrical way leads to the formation of a lithium-doped germanium nanowire. The positions of the lithium atoms are not random, as it has some stabilizing effect for the structure. This theoretical model rationalizes the present experimental observations.

The first member of this series is $\text{Ge}_{18}\text{Li}_6$ for which a C_s symmetric structure has been proposed. Structurally $\text{Ge}_{18}\text{Li}_6$ contains two *nido*- Ge_9 units surrounded by six lithium atoms. A Li acts as a bridging entity at the base of each *nido*- Ge_9 unit. The remaining four Li atoms are distributed around the Ge–Ge bond connecting the two *nido*-units. The optimized geometries are illustrated in Figure 13. The total energies and HOMO–LUMO gaps are listed in Table 7 and Table 8, respectively. $\text{Ge}_{18}\text{Li}_6$ possesses the largest HOMO–LUMO gap in the series, being 2.68 and 2.96 eV at B3LYP/ECP and B3LYP/SV(P), respectively.

Progressive addition of a Ge_9Li_5 unit results in a symmetrical growth pattern of the $\text{Ge}_{18}\text{Li}_6$ cluster to its next higher member $\text{Ge}_{27}\text{Li}_{11}$. Out of several other combinations considered, our computations resulted in this lowest-lying isomer. Structurally it falls under C_{2v} symmetry with three Ge_9 *nido*-units connected to each other in a linear fashion with Li atoms around it (cf.

Figure 13). This structure is characterized as an energy minimum with all real vibrational frequencies at the B3LYP/ECP level. Because of our computational limitations, however, it was not possible to carry out frequency analysis at B3LYP/SV(P) level. A similar building pattern leads to the formation of a chain-like $\text{Ge}_{36}\text{Li}_{16}$ which includes four *nido*- Ge_9 units and is surrounded by a number of lithium atoms. This structure falls under C_s symmetry, and the lithium atoms are distributed in a symmetrical way (cf. Figure 13). Again because of our computational limitations, vibrational frequency analyses were not possible on these structures. It has been demonstrated in the past^{20,21} that the lithium atom in Ge_n ($n = 2, 3$) units act as an electropositive entity. It has been proven that in smaller clusters the lithium atom always donates its electron to the germanium unit, providing the necessary electronic field to balance the charges.

5. Concluding Remarks

We have investigated the geometric and electronic structure as well as the growth pattern of the clusters Ge_nLi_m ($n = 4-5$, $m = 1-3$), Ge_nLi_m ($n = 6-8$; $m = 1, 2$), Ge_9Li_5 , $\text{Ge}_{18}\text{Li}_6$, $\text{Ge}_{27}\text{Li}_{11}$, and $\text{Ge}_{36}\text{Li}_{16}$. On the basis of our combined experimental and theoretical results, we are able to arrive at the following conclusions:

- (i) The Ge_nLi_m ($n = 4-5$, $m = 1-3$), and Ge_nLi_m ($n = 6-8$; $m = 1, 2$) clusters and the corresponding cations consistently possess low-spin ground state;
- (ii) The lowest-lying electronic states derived for the bare Ge_n clusters ($n = 4, 5, 6$) are in agreement with the ones reported earlier;
- (iii) For the neutral Ge_n ($n = 4-8$) clusters, singlet-triplet gaps of 21, 17, 16, 27, and 17 kcal/mol, respectively, are derived based on our B3LYP/aug-cc-pVDZ-pp computations;
- (iv) Doping with lithium atoms induces a considerable amount of structural changes of the parent structure, where the lithium atoms mainly act as bridging entities;
- (v) We were now able to propose a theoretical model which rationalizes the experimental spectrum of higher clusters. Accordingly, Ge_9Li_5 forms a unique structure. This structure is geometrically similar to three fused pentagonal Ge_5^- units with lithium atoms acting as bridging entities;
- (vi) In the case of $\text{Ge}_{18}\text{Li}_6$, $\text{Ge}_{27}\text{Li}_{11}$, and $\text{Ge}_{36}\text{Li}_{16}$ our proposed structures represent a growth pattern involving the Ge_9 units surrounded by lithium atoms, and this appears to be consistent with the mass spectrometric data.

We report for the first time the presence of oligomers of $[\text{Ge}_9]^{x-}$ units in a gas-phase experiment. From our combined experimental and theoretical analysis, we were able to derive a coupling pattern of lithium-doped germanium clusters similar to the one reported by Sevov et al.⁸ Accordingly, doping with lithium atoms enhances the stability of the Ge cluster where the former mainly act as charge balancer.

Acknowledgment. The authors are indebted to the Flemish Fund for Scientific Research (FWO-Vlaanderen), the Belgian Interuniversity Attraction Pole (IAP), and the KU Leuven Research Council (GOA and IDO programs) for continuing financial support.

Supporting Information Available: Experimental details. This material is available free of charge via the Internet at <http://pubs.acs.org>.

References and Notes

- (1) Kroto, H. W.; Heath, J. R.; Obrien, S. C.; Curl, R. F.; Smalley, R. E. *Nature* **1985**, *318*, 162.
- (2) Iijima, S. *Nature* **1991**, *354*, 56.
- (3) Jensen, K.; Weldon, J.; Garcia, H.; Zettl, A. *Nano Lett.* **2007**, *7*, 3508.
- (4) Chandrakumar, K. R. S.; Ghosh, S. K. *Nano Lett.* **2007**, *8*, 13.
- (5) Khlobystov, A. N.; Britz, D. A.; Briggs, G. A. D. *Acc. Chem. Res.* **2005**, *38*, 901.
- (6) Wang, X. Mass Spectrometric Study of Metal-Doped Group IV Clusters, Ph.D. Thesis, Department Natuurkunde en Sterrenkunde, Laboratorium Voor Vaste-Stoffysica en Magnetisme, K.U. Leuven, 2006.
- (7) Fässler, T. F. *Coord. Chem. Rev.* **2001**, *215*, 347. Spiekermann, A.; Hoffmann, S. D.; Kraus, F.; Fässler, T. F. *Angew. Chem., Int. Ed.* **2007**, *46*, 1638. King, R. B.; Silanghi-Dumitrescu, I. *Inorg. Chem.* **2003**, *42*, 6701. Koch, K.; Schnepf, A.; Schnöckel, H.; Anorg. Z. Allg. Chem. **2006**, *632*, 1710. Schenk, C.; Schnepf, A. *Angew. Chem., Int. Ed.* **2007**, *46*, 5315.
- (8) (a) Xu, L.; Sevov, S. C. *J. Am. Chem. Soc.* **1999**, *121*, 9245. Ugrinov, A.; Sevov, S. C. *J. Am. Chem. Soc.* **2002**, *124*, 10990. Ugrinov, A.; Sevov, S. C. *Inorg. Chem.* **2003**, *42*, 5789. Ugrinov, A.; Sevov, S. C. *C. R. Chimie* **2005**, *8*, 1878.
- (9) Pancharatna, P. D.; Hoffmann, R. *Inorg. Chem. Acta* **2006**, *359*, 3776.
- (10) Ugrinov, A.; Sevov, S. C. *Chem.—Eur. J.* **2004**, *10*, 3727.
- (11) Goicoechea, J. M.; Sevov, S. C. *Angew. Chem., Int. Ed.* **2005**, *44*, 4026.
- (12) Bouwen, W.; Thoen, P.; Vanhoutte, F.; Bouckaert, S.; Despa, F.; Weidele, H.; Silverans, R. E.; Lievens, P. *Rev. Sci. Instrum.* **2000**, *71*, 54.
- (13) Frisch, M. J., et al. Gaussian 03, Revision C.01, Gaussian, Inc., Wallingford, CT, 2004.
- (14) Ahlrichs, R.; Bär, M.; Häser, M.; Horn, H.; Kölmel, C. *Chem. Phys. Lett.* **1989**, *162*, 165.
- (15) Schaftenaar, G.; Noordik, J. H. *J. Comput.-Aided Mol. Des.* **2000**, *14*, 123.
- (16) Dennington, R., II.; Keith, T.; Millam, J.; Eppinnett, K.; Hovell, W. L.; Gilliland, R. GaussView, Version 3.0, Semichem, Inc., Shawnee Mission, KS, 2003.
- (17) Laaksonen, L. *J. J. Mol. Graph.* **1992**, *10*, 33. Bergman, D. L.; Laaksonen, L.; Laaksonen, A. *J. Mol. Graph. Model.* **1997**, *15*, 301.
- (18) Doye, J. P. K.; Wales, D. J. *J. Chem. Soc., Faraday Trans.* **1997**, *93*, 4233.
- (19) Johnston, R. L. *Dalton Trans.* **2003**, 4193.
- (20) Saunders, M. *J. Comput. Chem.* **2004**, *25*, 621.
- (21) Bera, P. P.; Sattelmeyer, K. W.; Saunders, M.; Schaefer, H. F., III.; Schleyer, P. v. R. *J. Phys. Chem. A* **2006**, *110*, 4287.
- (22) Gopakumar, G.; Lievens, P.; Nguyen, M. T. *J. Chem. Phys.* **2006**, *124*, 214312.
- (23) Gopakumar, G.; Lievens, P.; Nguyen, M. T. *J. Phys. Chem. A* **2007**, *111*, 4353.
- (24) Xu, W.; Zhao, Y.; Li, Q.; Xie, Y.; Schaefer, H. F., III. *Mol. Phys.* **2004**, *102*, 579.

JP900950K